

A Nonencapsulative Pendulum-Like Paper-Based Hybrid Nanogenerator for Energy Harvesting

Hongmei Yang, Mingming Deng, Qian Tang, Wencong He, Chenguo Hu, Yi Xi,*
Ruchuan Liu,* and Zhong Lin Wang*

The newly invented triboelectric nanogenerator (TENG) is deemed to be a more efficient strategy than an electromagnetic generator (EMG) in harvesting low-frequency (<2 Hz) water wave energy. Various TENGs with different structures and functions for blue energy have been developed, which can be roughly divided into two types: liquid–solid contact electrification TENGs and fully enclosed solid–solid contact electrification TENGs. Robustness and packaging are critical factors in the development of TENGs toward practical applications. Furthermore, for fully enclosed TENGs, the requirements and costs of packaging are very high, and they can be difficult to disassemble after enclosed, if there is something wrong with the devices. Herein, a nonencapsulative pendulum-like paper based hybrid nanogenerator for energy harvesting is designed, which mainly consists of three parts, one solar panel, two paper based zigzag multilayered TENGs, and three EMG units. This unique structure reveals the superior robustness and a maximum peak power of zigzag multilayered TENGs up to 22.5 mW is realized. Moreover, the device can be used to collect the mechanical energy of human motion in hand shaking. This work presents a new platform of hybrid generators toward energy harvesting as a portable practical power source, which has potential applications in navigation and lighting.

1. Introduction

Marine area covers more than 70% of the Earth's surface containing huge energy.^[1] Ocean, solar, and wind energy are the most familiar renewable and clean energies.^[2] Ocean energy is typically regarded as having five specific forms: tidal energy, water wave energy, ocean current energy, temperature gradient energy, and salinity gradient energy, among which ocean wave energy is one of the key directions of ocean energy


utilization.^[1,3] However, harvesting such energy is rather challenging due to the limitations of traditional electromagnetic generators (EMGs), especially at low frequency.^[4] How to harvest these types of energies with low cost, high stability, and high efficiency is the main barrier.

A triboelectric nanogenerator (TENG) based on the friction-induced and electrostatic induction effects has been proved to be a powerful invention technology for converting random and low-frequency mechanical energy into electricity with unique merits of high power density, high efficiency, light weight, low cost, and simple fabrication.^[1,4a,5] The TENG is much more effective than the EMG for harvesting energy in the frequency range of <5 Hz due to its distinct mechanism, which is ideally suited for our daily life and nature, such as the ocean waves.^[4a,b] Recently, various TENGs with different structures and functions for blue energy have been developed, which can be roughly divided into two types: liquid–solid contact electrification TENGs^[6] and fully enclosed solid–solid contact electrifi-

cation TENGs.^[7] However, robustness and packaging are critical factors for these TENGs toward practical applications, since the performance of TENG is greatly affected by environmental conditions, e.g., humidity.^[1,5c] What's more, for fully enclosed solid–solid contact electrification TENG, it is difficult to disassemble after being enclosed, if there is something wrong with the devices. In addition, with the seawater immersion and corrosion, the package will also fail soon; once water infiltrates the device, it will be unable to work, especially for electrical devices.

Dr. H. Yang, Dr. M. Deng, Dr. Q. Tang, Dr. W. He, Prof. C. Hu,
Prof. Y. Xi, Prof. R. Liu
State Key Laboratory of Power Transmission Equipment & System
Security and New Technology
Department of Applied Physics
School of Chemistry and Chemical Engineering
Chongqing University
Chongqing 400044, China
E-mail: yxi6@cqu.edu.cn, xiyi.xi@163.com; phyluirc@cqu.edu.cn

Prof. Y. Xi, Prof. Z. L. Wang
Beijing Institute of Nanoenergy and Nanosystems
Chinese Academy of Sciences
Beijing 100083, China
E-mail: zlwang@binn.cas.cn
Prof. Y. Xi, Prof. Z. L. Wang
School of Materials Science and Engineering
University of Science and Technology Beijing
Beijing 100083, China

 The ORCID identification number(s) for the author(s) of this article can be found under <https://doi.org/10.1002/aenm.201901149>.

DOI: 10.1002/aenm.201901149

Therefore, the requirement and cost of packaging are very high, and the difficulty coefficient is relatively large.

In this work, we fabricate a nonencapsulative pendulum-like paper-based hybrid nanogenerator for solar energy, water wave energy, and mechanical energy harvesting, which is operated with magnets by water wave. This hybrid nanogenerator mainly consists of three parts: one solar panel, two paper-based zigzag multilayered TENGs with four basic contact separation mode TENG units, and three EMG units. The integration of solar panel can add power supply and increase volume utilization of device effectively. Meanwhile, the triboelectric–electromagnetic hybrid structure broadens the working frequency ranges available as TENG can be more effective for low-frequency (<2 Hz) energy scavenging compared with EMG.^[1,4b,8] This unique structure reveals superior robustness (no obvious normalized current decay was found after continuously working for 800 000 cycles at 1 Hz) and a maximum peak power of zigzag multilayered TENGs up to 22.5 mW is realized. Moreover, combining with hand shaking, the device can be used to collect the mechanical energy of human motion. This work presents a new platform of hybrid generators toward multiple energy harvesting as a portable practical power source, which has the potential application for navigation and lighting.

2. Results and Discussion

2.1. Structural Design

The basic structure of the designed hybridized generator is presented in **Figure 1a**, which is composed of three parts: one commercially purchased solar panel on the top of the mover, two paper-based zigzag multilayered TENGs units with four basic contact separation mode TENGs on both sides of the mover, and three EMG units (three magnets were fixed on the bottom, front, and back sides of the mover and three copper coils were fixed to the corresponding bottom and both sides of the support, see details in the Experimental Section). Here, the solar cell panel is used to collect the solar energy for additional power output. One of the two magnets on the top of the mover is used to drive the device when the variable magnetic field is induced by the vibrated water wave energy in the ocean, and the other is used to maintain the balance of the device. **Figure 1b,c** show the photographs of the as-fabricated hybridized generator (the scale bar is 25 mm) and one paper-based zigzag multilayered TENG, respectively.

2.2. Schematics of Operating Principle

Based on the coupling effects of triboelectrification, electrostatic induction, and Faraday's law of electromagnetic induction,^[8] the working mechanism of the hybridized generator for converting mechanical energy into electricity can be illustrated in three consecutive steps in a full wobbled back and forth cycle as shown in **Figure 2**. The schematic diagram of working mechanism in **Figure 2a** and magnetic flux simulated by COMSOL in **Figure S1c** (Supporting Information) illustrate that when the device is wobbled back and forth by repulsive force between

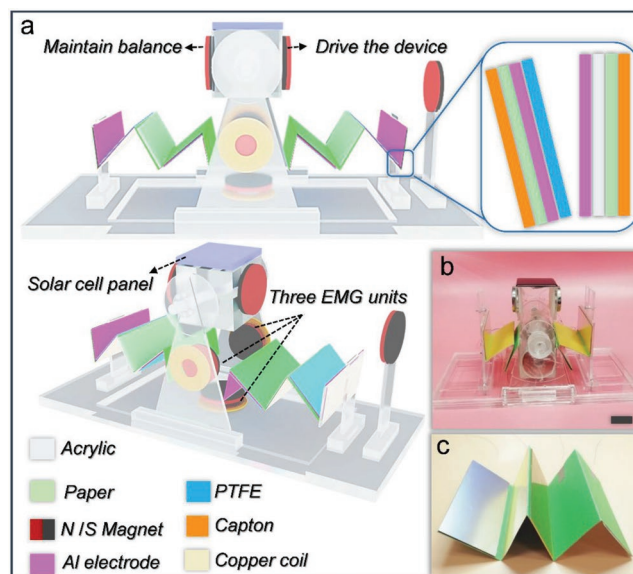


Figure 1. Structural design of the hybridized generator. a) Schematic diagram of the designed hybridized generator, which mainly consists of three parts: one solar panel, two zigzag multilayered TENGs with four basic units, and three EMG units (see **Figure 2a**), and the right part is the structure diagram for one basic TENG unit. b) Photograph of the as-fabricated hybridized generator; the scale bar is 25 mm. c) Photograph of one paper-based zigzag multilayered TENG.

magnets, both periodic trigger of zigzag multilayered TENG units is caused and magnetic flux is changed in copper coils to produce electrical output. The operation process of the device is similar to that of a pendulum model, while the paper-based zigzag multilayered TENG is similar to a spring oscillator. From the energy point of view, the variable magnetic field by water wave can compensate for the internal energy reduced by friction (such as air and bearing friction) during the swing of back and forth, thus converting water wave energy into electricity by this device. Moreover, from force and dynamics analysis as illustrated in **Figure S1b** (Supporting Information), the device is equivalent to a pendulum model. First, when the magnet moves up by water, the direction of the angular velocity vector by magnetic field force F_m is perpendicular to the paper face, and the device swings to the left. When the device moves to the leftmost end, the vertical acrylic baffle on the left will produce a right-facing elastic force F_e on the device, so the direction of the angular velocity vector is reversed, and the device wobbles back until to the rightmost end. At this moment, the vertical acrylic baffle on the right will produce a left-facing elastic force F_e on the device too, therefore, the device wobbles back and forth to convert water wave energy into electricity (see the details of working dynamic process by magnet in **Video S1** in the Supporting Information). **Figure 2b** shows the schematic illustrations of the charge distribution of one basic contact separation mode zigzag multilayered TENG unit. By conjunction of triboelectrification effect and electrostatic induction effect, physical contact between two different dielectric materials causes triboelectric charges on the two surfaces; a relative separation between the two dielectric materials by mechanical motion results in an electric potential drop across the two electrodes,

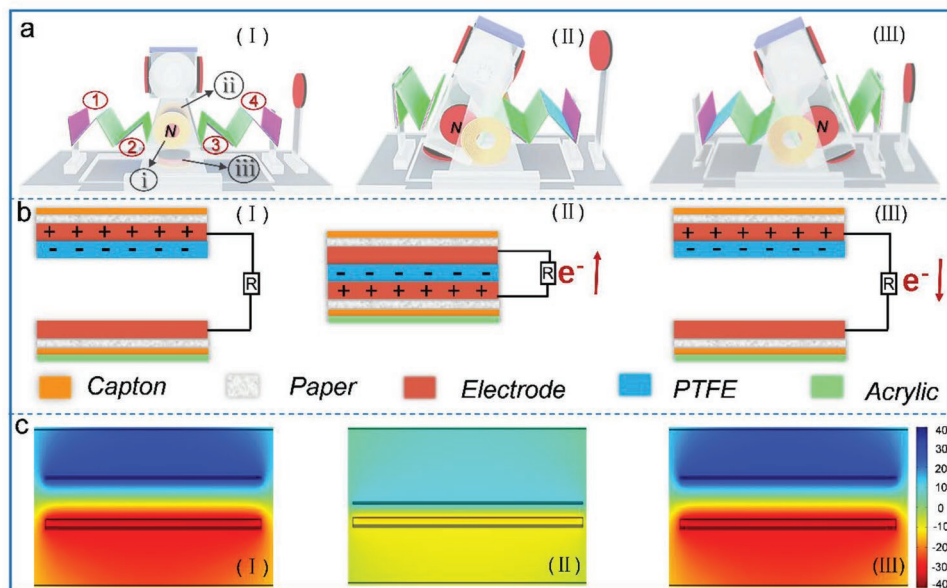


Figure 2. Schematics of the operating principle of the hybridized generator. a) The schematic diagram of working mechanism and the position of the four TENG units (1–4) and three EMG units (i–iii). b) Schematic illustrations of the charge distribution of one basic TENG unit. c) Potential distribution by COMSOL was employed to elucidate the working principle of TENG: (I) the initial state; (II) the intermediate state; (III) the final state.

which drives the electrons to flow between the two electrodes in order to balance the electrostatic system.^[5c] The voltage between the two electrodes for this contact-mode TENG can be given by^[9]

$$V = \frac{\sigma_1(z,t)d_1}{\epsilon_1} + \frac{[\sigma_1(z,t) - \sigma_c]z(t)}{\epsilon_0} \quad (1)$$

where σ_c is the saturated surface charge density due to friction in dielectric 1, $\sigma_1(z,t)$ is the charge density accumulated by free electrons in electrodes, d_1 is the thickness of the dielectric, $z(t)$ is the distance between dielectric layer and electrode, which is the periodic variable varying with time, and ϵ_1 and ϵ_0 are dielectric constants of dielectric and air, respectively, as shown in Figure S2 (Supporting Information). From Equation (1), we can see that periodic contact separation between dielectric layer and electrode is the process of converting mechanical energy into electrical energy. In addition, the variation of electric potential between two aluminum electrodes is also simulated via COMSOL, and the outcome is illustrated in Figure 2c.

2.3. Electric Output Performance

To investigate the features of hybridized generator for harvesting mechanical energy and solar energy, the relationship performance parameters of paper-based zigzag multilayered TENG, EMG, and solar cell panel have been systematically tested. First, in order to get optimal output performance of TENG part, the influence of factors, e.g., contact mode, the size of the paper, the position of removable ends, etc., is explored and the results are displayed in Figures S3 and S4 (Supporting Information). It can be seen that paper-based versus acrylic-based is the optimal contact mode among the four modes (Figure S3a, Supporting Information). For paper-based TENG,

the soft–hard contact mode can achieve the best contact. In addition, in the zigzag multilayered TENG, the acrylic layer can enhance the transfer charge to about 50 nC (Figure S3c, Supporting Information). It can be attributed to the fact that acrylic plate can strengthen the toughness of the paper and we can also consider the paper-based zigzag multilayered TENG as a spring oscillator, according to Hooke's law $F = kX$ (where k is the equivalent spring stiffness coefficient and X is the distance between compression and tension of the zigzag multilayered TENG), the existence of acrylic plate is similar to enhancing the stiffness coefficient of spring with a bigger force causing a fuller contact, so that it enhances the output. The paper with the thickness of 0.25 mm and width of 40 mm gets the largest transfer charge (Figure S3b,d, Supporting Information). Because the paper with different thicknesses and widths corresponds to different spring coefficients, only when the stiffness coefficient is appropriate, the best output characteristics can be obtained under the same driving force. What's more, the locations of the TENG and magnet on the vertical acrylic plates are investigated in Figure S4 (Supporting Information). It can be concluded that the zigzag multilayered TENG on the acrylic plate with $X = 0.5$ cm and $Y = 0.5$ cm (Figure S4c,d, Supporting Information) and magnet with $X = 2.5$ cm and $\Delta Y = 2.5$ cm (Figure S4e,f, Supporting Information) is optimum working state of the device with 251 nC. Herein, the hybrid generator for harvesting mechanical energy in harsh environment is designed with the optimal parameters displayed in Figure 1.

A microstep driver was used to quantitatively investigate the electrical output characterization of the hybrid generator and the outputs are shown in Figure 3 and Figure S5 (Supporting Information). The locations of four TENG units and three EMG units are illustrated in Figure 2a(I). For contact separation mode TENG, at open-circuit condition, there is no charge

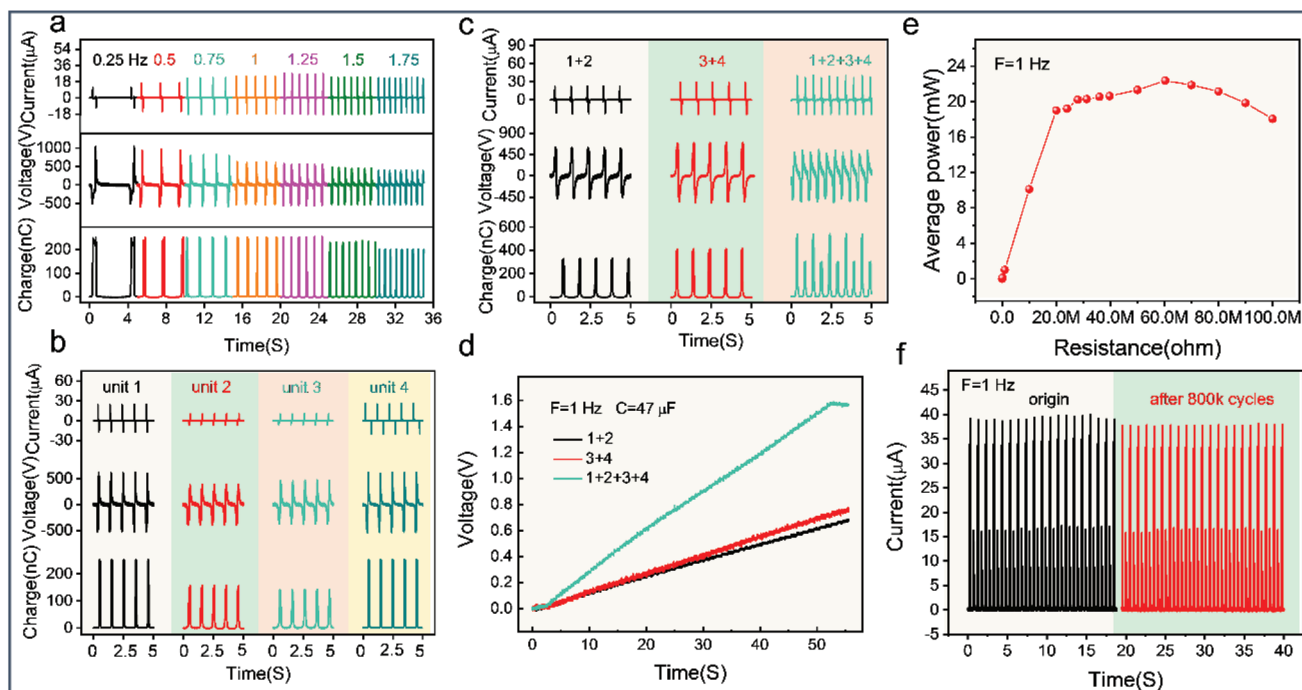


Figure 3. Electrical output characterization of zigzag multilayered TENG driven by a microstep driver for quantitative investigation. a) The short-circuit current (I_{sc}), open-circuit voltage (V_{oc}) (the logic circuit is shown in Figure S6a in the Supporting Information), and transfer charge of unit 1 (see Figure 2a(b)) for working frequency ranging from 0.25 to 1.75 Hz. b) I_{sc} , V_{oc} , and transfer charge of every unit. c) I_{sc} , V_{oc} , transfer charge, and d) measured voltages of a 47 μF capacitor charged by TENG with different configurations of units 1, 2, 3, and 4. e) Average power and resistance of external load. f) Robustness test of zigzag multilayered TENG. The working frequency is 1 Hz.

transfer, and Q is 0. Therefore, the open-circuit voltage V_{oc} is given by^[10]

$$V_{oc} = \frac{\sigma_c Z(t)}{\epsilon_0} \quad (2)$$

At short-circuit condition, V is 0. Therefore, the transferred charges are

$$Q_{sc} = \frac{S\sigma_c Z(t)}{d_0 + Z(t)} \quad (3)$$

$$I_{sc} = \frac{dQ_{sc}}{dt} = \frac{S\sigma_c d_0 V(t)}{(d_0 + Z(t))^2} \quad (4)$$

Here, S is the contact area of tribolayer, $d_0 = d_1/\epsilon_1$, and $V(t)$ is the speed of contact separation between dielectric layer and electrode. Figure 3a shows the frequency (0.25–1.75 Hz) dependence of short-circuit current (I_{sc}), open-circuit voltage (V_{oc}) (see the test circuit diagram in Figure S6a in the Supporting Information), and transfer charge of unit 1 of paper-based zigzag multilayered TENG. It can be seen that as the frequency increases, V_{oc} gradually decreases from 1061.6 to 417.5 V and transfer charge gradually decreases from 254 to 202 nC, and when the frequency is less than 1.25 Hz, the transfer charge keeps a stable value of 254 nC, which is the result of insufficient contact causing reduction of σ_c with increasing frequency. In contrast, I_{sc} increases gradually from 11.4 to 22.5 μA and the maximum value of 27.7 μA is obtained at 1.25 Hz. The

reason is that current is the ratio of transfer charge to time and $V(t)$ increases with the frequency. The output performances of every TENG unit are exhibited in Figure 3b. It indicates that the output performance of four units is symmetrical. The two units near the two ends are larger than the two units in the middle. We can consider that the contact separation time of the two TENG units in one zigzag multilayered TENG is the same, and the contact separation distance of the two TENG units near the ends is larger than that of the two units in the middle; therefore, $V(t)$ of the two units near the ends is larger than that of the two units in the middle due to a larger output according to Equations (2)–(4). Furthermore, for two units of one paper-based zigzag multilayered TENG, they have the same phase, so that their output signals can be superimposed as shown in Figure 3c. It can be seen that the superimposed signals of two units are enhanced and compensated compared with Figure 3b (I_{sc} increases from 26.2 to 29.7 μA , V_{oc} increases from 613 to 695 V, and transfer charge increases from 253 to 416 nC). When the four units are superimposed together in parallel, it indicates that I_{sc} increases from 29.7 to 41.3 μA while V_{oc} decreases from 695 to 567 V. Transfer charges of two zigzag multilayered TENG units in one side increase from 416 to 551 nC, while those of other two units decrease from 416 to 308 nC. It is because that for the two zigzag multilayered TENGs, their phase is not exactly opposite, leading to the enhancement of one part and the weakening of another part. Overall, the energy density of the output is enhanced. Figure 3d illustrates the measured voltages of a 47 μF capacitor charged

by zigzag multilayered TENG with different unit configurations (see circuit diagrams in Figure S6b in the Supporting Information). For the integration with four units, the capacitor can be charged to 1.6 V within 1 min, which indicates the superior integration of the device and further improvements in the electric output could be accomplished by integrating more units. Figure 3e displays the output power of the TENG when various external loads (from 1 k Ω to 100 M Ω) are applied. The maximum power output is obtained at 60 M Ω , corresponding to a peak power of 22.5 mW with four units. On the other hand, the reliability of the device, primarily represented by its output stability and mechanical durability, is another crucial feature in applications. According to the rectified I_{sc} of TENG part before and after continuously working for 800 000 cycles in Figure 3f, it can be seen that no obvious normalized current decay is found after continuously working for a long time, which indicates the satisfactory mechanical durability of the device. These results were obtained at a fixed working frequency of 1 Hz driven by a microstep driver. Furthermore, in order to investigate the effect of salinity and humidity on the output performance of TENG, we simulated the salinity conditions of the ocean with 3.5% NaCl solution and the different humidity values for the output performances of TENG are shown in Figure S7 (Supporting Information). Figure S7a (Supporting Information) illustrates that the output voltage of seawater condition is about 80% of that of tap water with the relative humidity of 85%. The reason is that ions in brine, such as chloride ion, are carried into the air as water molecules evaporate, neutralizing part of the surface charge of the friction material, resulting in a reduction of electrical output performance of TENG. The relationship between normalized voltage and relative humidity with 3.5% NaCl solution is illustrated in Figure S7b (Supporting Information), it indicates a gradual decrease in output with the increase of relative humidity as the profusion of water molecules in moisture atmosphere can extremely reduce the triboelectric charges on the surface of frictional/dielectric materials and result in the reduction of electrical output performance of TENGs.^[11] In order to avoid the influence of humidity and salinity on the output of the device, we simply encapsulated and isolated the main part of the device with preservative film without affecting the operation of the device (as shown in Figure S7c in the Supporting Information), the output performance is shown in Figure S7c (Supporting Information). It demonstrates that a stable performance is attained in different relative humidity environments. Compared with the process of full encapsulation (waterproof) in water, this kind of encapsulation treatment has the advantages of simple process, low cost, and much less difficulty. In addition, it is also much easier to reassemble devices if there is something wrong or friction materials need to be replaced.

For the EMG unit, according to Faraday's law, the open-circuit voltage (V_{oc}) and the short-circuit current (I_{sc}) can be expressed as

$$V_{oc} = -N \frac{d\Phi}{dt} \quad (5)$$

$$I_{sc} = -\frac{V_{oc}}{R} \quad (6)$$

where Φ is the total magnetic flux in each coil, N is the number of turns in the copper coil, and R represents the internal resistance of the coil. Apparently, the variation rate of the magnetic flux is related to the frequency. The electrical outputs of EMG are displayed in Figure S5 (Supporting Information). For unit (i) in Figure S5a (Supporting Information), it is observed that the amplitudes of I_{sc} (from ≈ 1.5 to 6.3 mA) and V_{oc} (from ≈ 0.25 to 1.1 V) increase with an increase of working frequency ranging from 0.5 to 2.5 Hz. The performance of I_{sc} and V_{oc} for both EMG units at the symmetrical positions (Figure S5b, Supporting Information) is similar with a stable electric output of $V_{oc} \approx 0.42$ V and $I_{sc} \approx 2.65$ mA. However, because the distance between magnet and coil of unit (iii) is different from the other two units, unit (iii) gives the largest electric output of $V_{oc} \approx 0.98$ V and $I_{sc} \approx 6.2$ mA. What's more, the electrical output with different configurations of units (i), (ii), and (iii) in series (Figure S5c, Supporting Information) shows an I_{sc} of ≈ 3.65 mA and a V_{oc} of ≈ 1.8 V, demonstrating the excellent phase synchronization of EMG units. It can be concluded that the maximum power output of EMG with three units in series on the resistance of the external load was obtained at 480 Ω , with a peak power of 1.39 mW at a frequency of 1 Hz from Figure S5d (Supporting Information). These results were obtained at a fixed working frequency of 1 Hz driven by a microstep driver.

Figure 4a illustrates I_{sc} (≈ 34 μ A and 3.5 mA) and V_{oc} (≈ 491 and 1.74 V) for TENG and EMG by water wave, respectively, and the experimental setup is shown in Figure 5a. A 47 μ F capacitor was used to detect the power supply capability of TENG and EMG when the device was driven by water wave. It can be charged to 4.3 V by two parts in parallel in less than 1 min, as shown in Figure 5b (see wire connection in Figure S6c in the Supporting Information). For the triboelectric–electromagnetic hybrid nanogenerator, it is worth noting that the initial charging rate of EMG is faster than that of TENG, because the output current of EMG is much larger than that of TENG, so the voltage in initial charging is mainly contributed by EMG, and when the voltage reaches the EMG value of about 1.74 V, the capacitor is mainly charged by TENG. The picture in Figure 5c shows that this device can convert the water wave energy into electricity available to power electronics, such as more than 220 light-emitting diodes (LEDs), as shown in Video S3 (Supporting Information), revealing the potential of application in blue energy. The time–current and time–voltage signals of the solar panel are displayed in Figure 4c with 72.5 mA and 6.9 V. It could drive a thermohygrometer continuously when the Xenon light source was used, as shown in Figure 5d and Video S2 (Supporting Information) (see wire connection in Figure S6d in the Supporting Information). Moreover, combining with hand shaking, the device can be used to collect the energy of hand motion, and an electronic vernier caliper is driven successfully (see illustration of wire connection in Figure S6d in the Supporting Information). Here, a 47 μ F capacitor is used as energy storage device and the photograph of the hand-driven generator is shown in Figure 4f. This hybrid device manifests the ability to convert multiple energies into electricity as a portable practical power source.

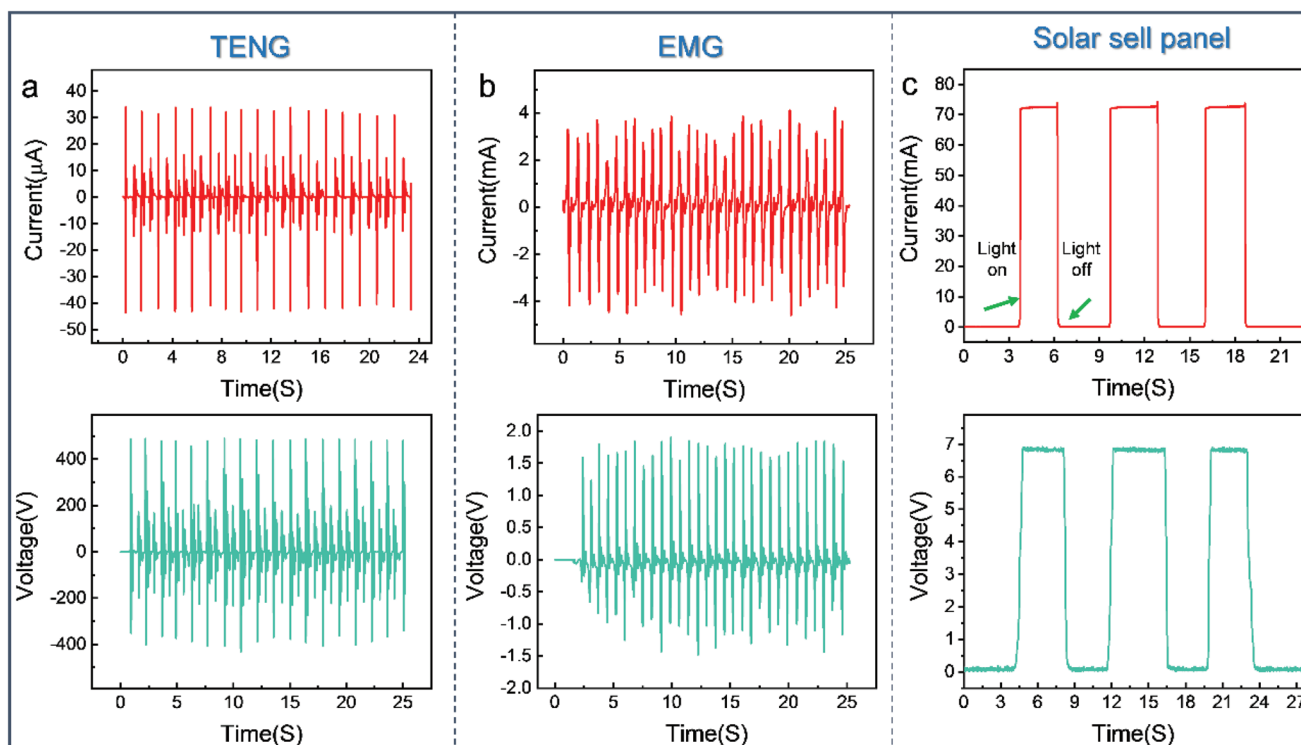


Figure 4. Electrical output performance characterization of the hybridized generator. a,b) I_{sc} and V_{oc} for TENG and EMG by water wave, respectively. c) The time–current and time–voltage signals of the solar panel.

3. Conclusion

We have designed a nonencapsulative pendulum-like paper-based hybrid nanogenerator for water wave energy, mechanical

energy, and solar energy harvesting. The design of the unique structure broadens the working frequency ranges available, avoids the influence of performance by harsh underwater environment conditions, and reveals superior robustness. It avoids

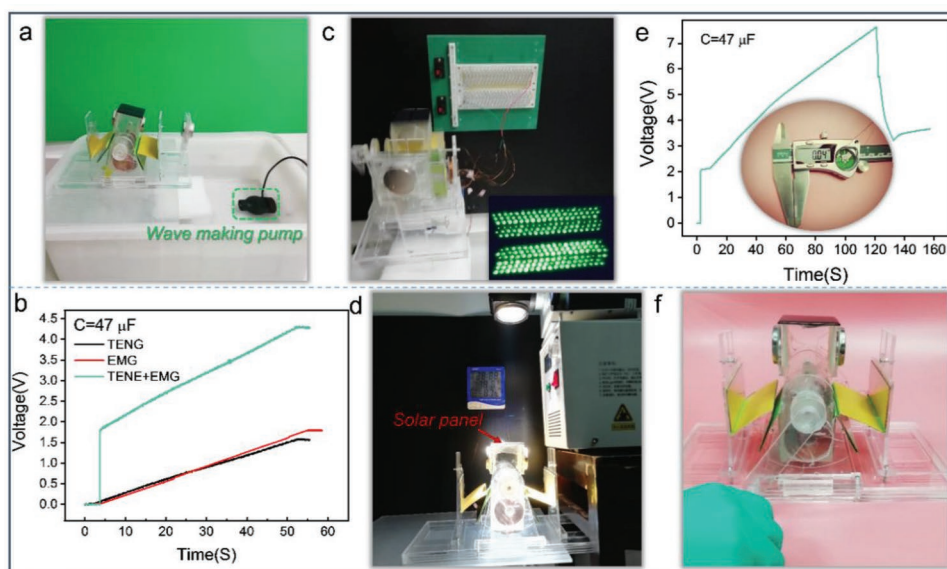


Figure 5. Demonstrations of the hybridized generator as a practical power source. a) Photograph of experimental setup. b) Measured voltages of a 47 μF capacitor charged by TENG, EMG, and TENG + EMG, respectively. c) Demonstrations of the device for collecting water wave energy, the insert picture shows the LEDs lighted by TENG part. d) Photograph of thermohygrometer that was continuously powered by the solar panel. e) Measured voltages of a 47 μF capacitor charged by TENG + EMG parts by hands; the insert picture shows a digital vernier caliper driven by it. f) Photograph of the hand-driven generator.

the difficulties in packaging and disassembling for repairmen while harvesting blue energy effectively. Moreover, the broad frequency ranges of the device enable it to collect the mechanical energy of human motion as well as other mechanical activities. This work presents a new platform of hybrid generators toward multiple energy harvesting as a portable practical power source, which has the potential applications for navigation and lighting.

4. Experimental Section

Fabrication of TENG Part: First, stick a single layer of Capton tape with a thickness of 0.05 mm on the back of the paper (length, L : 20 cm; width, W : 10 cm; thickness, T : 0.25 mm) to enhance the robustness of the paper. Then, fold paper into zigzag shape as shown in Figure 1c. Acrylic plate (L : 10 cm; W : 4 cm; T : 1 mm) integrated with an aluminum film (T : 0.01 mm) was attached to one side of paper as one tribolayer and electrode, and an aluminum (T : 0.01 mm) film and polytetrafluoroethylene film (T : 0.05 mm) with the same size were stuck on the another side of paper as another electrode and tribolayer, respectively, to fabricate a basic contact separation mode TENG unit (see structure diagram in the right amplification of Figure 1a). The TENG part contained two zigzag multilayered TENGs with four basic units. It is worth mentioning that at the connection of two basic units of one zigzag multilayered TENG, there existed an acrylic plate (L : 10 cm; W : 4 cm; T : 1 mm) to increase the contact intensity of TENG. The frame of the whole device was composed of acrylic plate cut by laser cutting machine, bearing, and stainless steel rod. Finally, one side of the zigzag multilayered TENG was fixed on the vertical acrylic plate, which can be adjusted horizontally and vertically, and another side was fixed on the mover, as shown in Figure 1a.

Fabrication of EMG Part: Three magnets with a diameter of 40 mm were installed on the two sides and the bottom of the mover, and three copper coils (1500 laps, 0.018 mm diameter of copper wire) were installed on the two vertical acrylic stents and the top of the bottom frame aligned well with three magnets working as EMG part. Moreover, two magnets with a diameter of 40 mm and a commercially purchased solar cell panel (rated voltage: 8 V; rated current: 80 mA) with the size of 27.5 cm² were installed on the top of the mover. Here, one of the magnet was used to drive the device, and another was used to maintain the balance of device, and the solar cell panel was used to collect the solar energy. When the device was wobbled back and forth by external force, the working cycles of TENG units were caused and magnetic flux was varied in copper coils to produce electrical output.

Measurement and Characterization: The output signals of the hybrid device were measured by a voltage preamplifier (Keithley 6514 System Electrometer). The software platform was constructed based on LabVIEW, which was capable of realizing real-time data acquisition and analysis. The potential distribution in the TENG and magnetic flux in the EMG were calculated from a finite-element simulation using COMSOL Multiphysics software. During the testing process, a microstep driver (MA860H) was utilized to provide a reciprocating motion with different frequencies. A xenon light source (solar-500) and wave making pump were used to simulate sunlight and water wave, respectively.

Supporting Information

Supporting Information is available from the Wiley Online Library or from the author.

Acknowledgements

This work was supported by the National Key R&D Project from Ministry of Science and Technology (2016YFA0202704), the National Natural

Science Foundation of China (51772036 and 51572040), the Fundamental Research Funds for the Central Universities (2019CDXZWL001 and 2018CDJDWL0011), National Key Research and Development Programs—Intergovernmental International Cooperation in Science and Technology Innovation Project (grant no. 2016YFE0111500), and the large-scale equipment sharing fund of Chongqing University.

Conflict of Interest

The authors declare no conflict of interest.

Keywords

hybrid triboelectric nanogenerators, multiple energy harvesting, nonencapsulation

Received: April 8, 2019

Revised: June 24, 2019

Published online:

- [1] Z. L. Wang, T. Jiang, L. Xu, *Nano Energy* **2017**, *39*, 9.
- [2] a) A. Mohammadi, M. Mehrpooya, *Energy* **2018**, *158*, 632; b) H. Guo, X. He, J. Zhong, Q. Zhong, Q. Leng, C. Hu, J. Chen, L. Tian, Y. Xi, J. Zhou, *J. Mater. Chem. A* **2014**, *2*, 2079; c) Z. Wen, M.-H. Yeh, H. Y. Guo, J. Wang, Y. Zi, W. D. Xu, J. Deng, L. Zhu, X. Wang, C. G. Hu, L. Zhu, X. Sun, Z. L. Wang, *Sci. Adv.* **2016**, *2*, e1600097; d) W. Wang, Y. Wu, Z. Chang, F. Chen, H. Wang, G. Gu, H. Zheng, G. Cheng, Z. L. Wang, *ACS Appl. Mater. Interfaces* **2019**, *11*, 6396; e) L. Zhu, P. Lin, B. Chen, L. Wang, L. Chen, D. Li, Z. L. Wang, *Nano Res.* **2018**, *11*, 3877; f) Y.-C. Lai, Y.-C. Hsiao, H.-M. Wu, Z. L. Wang, *Adv. Sci.* **2019**, *6*, 1801883; g) C. Zhao, Q. Zhang, W. Zhang, X. Du, Y. Zhang, S. Gong, K. Ren, Q. Sun, Z. L. Wang, *Nano Energy* **2019**, *57*, 440; h) J. Wang, W. Ding, L. Pan, C. Wu, H. Yu, L. Yang, R. Liao, Z. L. Wang, *ACS Nano* **2018**, *12*, 3954.
- [3] S. Draycott, B. Sellar, T. Davey, D. R. Noble, V. Venugopal, D. M. Ingram, *Renewable Sustainable Energy Rev.* **2019**, *104*, 15.
- [4] a) Y. Zi, H. Guo, Z. Wen, M. H. Yeh, C. Hu, Z. L. Wang, *ACS Nano* **2016**, *10*, 4797; b) F. R. Fan, W. Tang, Y. Yao, J. Luo, C. Zhang, Z. L. Wang, *Nanotechnology* **2014**, *25*, 135402.
- [5] a) F.-R. Fan, Z.-Q. Tian, Z. L. Wang, *Nano Energy* **2012**, *1*, 328; b) H. Yang, W. Liu, Y. Xi, M. Lai, H. Guo, G. Liu, M. Wang, T. Li, X. Ji, X. Li, *Nano Energy* **2018**, *47*, 539; c) Z. L. Wang, *Faraday Discuss.* **2014**, *176*, 447; d) C. Wu, A. C. Wang, W. Ding, H. Guo, Z. L. Wang, *Adv. Energy Mater.* **2019**, *9*, 1802906; e) X. Pu, H. Guo, J. Chen, X. Wang, Y. Xi, C. Hu, Z. Wang, *Sci. Adv.* **2017**, *3*, e1700694.
- [6] a) X. J. Zhao, G. Zhu, Y. J. Fan, H. Y. Li, Z. L. Wang, *ACS Nano* **2015**, *9*, 7671; b) X. J. Zhao, J. J. Tian, S. Y. Kuang, H. Ouyang, L. Yan, Z. L. Wang, Z. Li, G. Zhu, *Adv. Mater. Interfaces* **2016**, *3*, 1600187; c) M. Xu, S. Wang, S. L. Zhang, W. Ding, P. T. Kien, C. Wang, Z. Li, X. Pan, Z. L. Wang, *Nano Energy* **2019**, *57*, 574; d) Z.-H. Lin, G. Cheng, W. Z. Wu, K. C. Pradel, Z. L. Wang, *ACS Nano* **2014**, *8*, 6440; e) L. Pan, J. Wang, P. Wang, R. Gao, Y.-C. Wang, X. Zhang, J.-J. Zou, Z. L. Wang, *Nano Res.* **2018**, *11*, 4062.
- [7] a) H. Yang, M. Wang, M. Deng, H. Guo, W. Zhang, H. Yang, Y. Xi, X. Li, C. Hu, Z. Wang, *Nano Energy* **2019**, *56*, 300; b) H. Guo, Z. Wen, Y. Zi, M.-H. Yeh, J. Wang, L. Zhu, C. Hu, Z. L. Wang, *Adv. Energy Mater.* **2016**, *6*, 1501593; c) B. D. Chen, W. Tang, C. He, C. R. Deng, L. J. Yang, L. P. Zhu, J. Chen, J. J. Shao, L. Liu, Z. L. Wang, *Mater. Today* **2018**, *21*, 88; d) Y. Xi, J. Wang, Y. Zi, X. Li, C. Han, X. Cao, C. Hu, Z. Wang, *Nano Energy* **2017**, *38*, 101; e) X. Liang, T. Jiang, G. Liu, T. Xiao, L. Xu, W. Li, F. Xi, C. Zhang,

- Z. L. Wang, *Adv. Funct. Mater.* **2019**, 1807241, <https://doi.org/10.1002/adfm.201807241>; f) Y. Xi, H. Guo, Y. Zi, X. Li, J. Wang, J. Deng, S. Li, C. Hu, X. Cao, Z. L. Wang, *Adv. Energy Mater.* **2017**, 7, 1602397; g) X. Wang, S. Niu, Y. Yin, F. Yi, Z. You, Z. L. Wang, *Adv. Energy Mater.* **2015**, 5, 1501467; h) T. Jiang, Y. Yao, L. Xu, L. Zhang, T. Xiao, Z. L. Wang, *Nano Energy* **2017**, 31, 560; i) L. Xu, T. Jiang, P. Lin, J. J. Shao, C. He, W. Zhong, X. Y. Chen, Z. L. Wang, *ACS Nano* **2018**, 12, 1849; j) P. Cheng, H. Guo, Z. Wen, C. Zhang, X. Yin, X. Li, D. Liu, W. Song, X. Sun, J. Wang, Z. L. Wang, *Nano Energy* **2019**, 57, 432.
- [8] C. Zhang, W. Tang, C. B. Han, F. R. Fan, Z. L. Wang, *Adv. Mater.* **2014**, 26, 3580.
- [9] a) Z. L. Wang, *Mater. Today* **2017**, 20, 74; b) S. Niu, Z. L. Wang, *Nano Energy* **2015**, 14, 161.
- [10] S. Niu, S. Wang, L. Lin, Y. Liu, Y. S. Zhou, Y. Hu, Z. L. Wang, *Energy Environ. Sci.* **2013**, 6, 3576.
- [11] K. Y. Lee, J. Chun, J. H. Lee, K. N. Kim, N. R. Kang, J. Y. Kim, M. H. Kim, K. S. Shin, M. K. Gupta, J. M. Baik, S. W. Kim, *Adv. Mater.* **2014**, 26, 5037.